Supporting Material

Mechanistic investigation of the arrhythmogenic role of oxidized CaMKII in the heart

Panagiota T. Foteinou[1], Joseph L. Greenstein[1], and Raimond L. Winslow[1]*

[1]Institute of Computational Medicine and Department of Biomedical Engineering, Johns Hopkins University, Baltimore, MD, USA

***Correspondence:** Raimond L. Winslow, Institute of Computational Medicine, Johns Hopkins University, Baltimore, MD, USA.
rwinslow@jhu.edu

Model Description

Changes to the Ca^{2+}/CaM Model (dyad)

In the ordinary differential equation (ODE) model of Chiba et al. (1), the binding reaction between Ca^{2+} and CaM is computed deterministically using the sequential four-step Ca^{2+} binding model of Holmes et al. (2). This model includes cooperative Ca^{2+} binding within each CaM lobe (C-terminal and N-terminal lobe) and assumes that the C-terminal Ca^{2+} binding sites are occupied before the N-terminal sites. CaM binds two Ca^{2+} ions to its C-terminal lobe with a high affinity (K_d of ~1-2 μM) and two Ca^{2+} ions to its N-terminal lobe with a low affinity (K_d of ~2.6-13 μM). It is therefore expected that CaM will bind four Ca^{2+} ions in the presence of high Ca^{2+} concentration ($[Ca^{2+}]$) (e.g. at sites of Ca^{2+} release where $[Ca^{2+}]_{dyad}$ is relatively high) forming the fully Ca^{2+}-bound CaM ($CaMCa_4$). Predicated upon this, we simplified the four-step Ca^{2+}/CaM binding scheme to a one-step process (Eq. S1) by assuming that all reactions in the dyadic cleft rapidly reach equilibrium.

$$\left[\mathrm{CaMCa_4}\right]_{\mathrm{dyad}} = \frac{1}{K_{d,app}} \cdot \left[Ca^{2+}\right]^4_{\mathrm{dyad}} \cdot \left[\mathrm{CaM_{free}}\right]_{\mathrm{dyad}}$$

$$K_{d,app} = \left(\frac{k_{-1}}{k_1}\right) \cdot \left(\frac{k_{-2}}{k_2}\right) \cdot \left(\frac{k_{-3}}{k_3}\right) \cdot \left(\frac{k_{-4}}{k_4}\right) \qquad \text{(S1)}$$

$$\left[\mathrm{CaM_{free}}\right]_{\mathrm{dyad}} = \frac{\mathrm{CaM_{total}}}{1 + \left(\frac{k_1}{k_{-1}} \cdot \left[Ca^{2+}\right]_{\mathrm{dyad}}\right) \cdot \left(1 + \frac{k_2}{k_{-2}} \cdot \left[Ca^{2+}\right]_{\mathrm{dyad}} + \frac{k_2 \cdot k_3}{k_{-2} \cdot k_{-3}} \cdot \left[Ca^{2+}\right]^2_{\mathrm{dyad}} + \frac{k_2 \cdot k_3 \cdot k_4}{k_{-2} \cdot k_{-3} \cdot k_{-4}} \cdot \left[Ca^{2+}\right]^3_{\mathrm{dyad}}\right)}$$

All kinetic rate constants (e.g. k_{-1}, k_{-2}, k_{-3}, k_{-4} …k_1, k_2, k_3, k_4) have values in agreement with those reported previously (1) as shown in **Tables S1** and **S2**. As shown in **Fig. S3,** for high $[Ca^{2+}]_{dyad}$ (e.g. > 25 μM) consistent simulation results for $[CaMCa_4]$ are obtained both with the

four-step Ca^{2+} binding scheme of Chiba et al. (1) and the proposed simplified Ca^{2+}/CaM scheme. For lower [Ca^{2+}] (e.g. cytosolic $[Ca^{2+}]_i$), the equilibrium approximation is no longer valid and therefore we employed the four-step Ca^{2+}/CaM binding scheme of Chiba et al. (1) without any further modification.

Changes to the model of Hashambhoy et al. (3)

The following changes were made to the model of Hashambhoy et al. (3):

1. The CaMKII activation model of Hashambhoy et al. (3) is replaced by our new CaMKII model that includes both the phosphorylation-dependent activation pathway and the newly identified oxidation-dependent activation pathway. The activity of a single CaMKII holoenzyme is defined as in the original model of Hashambhoy et al. (4).
2. In order to obtain physiologically relevant I_{CaL} facilitation (**Fig. S4A)**, the LCC dephosphorylation rate is reduced by a factor of 2. This parameter (new value 0.6 units PP2A x (units CaMKII)$^{-1}$) controls the peak I_{CaL} simulated in the I_{CaL} facilitation (voltage clamp) protocol as illustrated in **Fig. S4A**. This value is similar to that originally published by Hashambhoy et al (4).
3. The mode 2 mean open time is reduced from 10 ms to 6 ms which lies within the experimental range of 5 to 10 ms (5, 6). This reduction is achieved by scaling the mode 2 rate of LCC closing by 1.67 as compared to that of Hashambhoy et al. (3).With this new value, the model has a 12-fold reduction in the LCC closing rate for mode 2 versus mode 1. This adjustment was necessary to obtain stable action potentials.
4. Following incorporation of the proposed CaMKII activation model into our canine cardiac myocyte model (3), the conductance of I_{Kr} (G_{Kr}) is increased by 70%. This scaling was derived from recent experimental data of Szabo et al. (7). These data indicate a far greater density of I_{Kr} (e.g. 0.8 pA/pF) at depolarized test potentials (e.g. + 40 mV) than those measured in earlier studies. As a result of this change, the model simulates a peak I_{Kr} density = 0.5 pA/pF at 1 s PCL pacing which is consistent with the reported experimental value of 0.55 pA/pF (8).
5. Minor adjustments were made to the SR Ca^{2+} pump cycling rate (15% increase) and the density of I_{NCX} (12% increase) to ensure normal Ca^{2+} transient properties ($\Delta[Ca^{2+}]_i$ ~ 0.8 μM) at 1 s PCL pacing.
6. The rate of RyR dephophosphorylation ($k_{RyRDephosph}$) is constrained such that during 2 s PCL pacing, the RyR phosphorylation levels match those measured experimentally (9). By increasing $k_{RyRDephosph}$ from its original value of 0.000952 ms^{-1} to 0.0019 ms^{-1}, the model simulates 8% RyR phosphorylation as reported in the experiments.
7. The parameter that represents Ca^{2+} sensitivity in the opening rate of phosphorylated RyRs (Ca_{shift}) is increased from 1.3 to 1.35. This change is validated by simulating the Ca^{2+} spark frequency (CaSpF) protocols of Guo et al. (10) in the absence of PLB (see **Methods** section). Under this condition, the model yields a 99% increase in CaSpF which is in agreement with the reported experimental value of 98%.

8. All transition rates of the Na^+ channel Markov model are replaced with those previously published by Grandi et al. (11) with the exception of the control (WT) value of the rate α_8, which is reduced from 4.7 x 10^{-7} ms^{-1} to 3.2 x 10^{-7} ms^{-1}. Using this new rate, the model simulates a physiologically accurate late I_{Na} (I_{NaL}) under the voltage clamp protocol of Wagner et al. (12) (simulated value is 0.13% of peak I_{Na} consistent with the experimental range 0.23 ± 0.1%).

Modeling the effects of H_2O_2 on I_{NaL}

A key limitation of the cardiac Na^+ channel model is that dynamic CaMKII-mediated phosphorylation of the protein is not modeled. Modeling this reaction would require kinetic data for reactions rates which are not yet available. In order to simulate the CaMKII dependent effect of H_2O_2 on I_{NaL}, the rate a_8 is increased such that the model reproduces the relevant experimental data (13). To elicit I_{NaL}, myocytes were voltage-clamped from a holding potential of -120 mV to a test potential of -30 mV for 1000-ms under both control and oxidative stress conditions (200 µM H_2O_2). By increasing a_8 from 3.2 x 10^{-7} (control or WT condition) to 5.4 x 10^{-7} ms^{-1} (oxidative stress condition) the total Na^+ charge transported (integral of I_{NaL}) between 50 and 500 ms after onset of the test pulse before and during H_2O_2 exposure is -163.89 pC/µF and -271.83 pC/µF, respectively. These values lie in general agreement with the reported experimental values: -203.5 ± 21 (WT) and -380.1 ± 101.1 pC/µF (200 µM H_2O_2) (13).

Modeling the effects of H_2O_2 on CaMKII-PP1

Using both experimental in vivo and in vitro ischemia models, O'Loghlen et al. (14) demonstrated that protein phosphatase 1 (PP1) activity is inhibited upon H_2O_2-treatment which results in increased target phoshorylation levels; however, the mechanisms underlying this observation remain unknown. To explore the potential role of oxidative stress on CaMKII dephosphorylation rate due to PP1 inhibition, we have introduced an inhibitory constant (K_{mROS}) in the catalytic rate of PP1 (k_{cat_PP1}) defining a new parameter ($k_{cat\_PP1}^{new}$) as follows:

$$k_{cat\_PP1}^{new} = \frac{k_{cat\_PP1}}{1 + \frac{[H_2O_2]}{K_{mROS}}}$$

For low values of K_{mROS} (e.g. 0.1 mM) and increased oxidative stress ($[H_2O_2]$ = 1 mM) (**Fig. S5)**, the model predicts significant CaMKII autophosphorylation which is consistent with the experimental evidence from Song et al. (15). Without this inhibitory constant, the model is unable to reproduce the experimentally observed degree of CaMKII autophosphorylation.

Equation Rates and Parameters

Most of the rates of the stochastic CaMKII model are identical to those published previously by Chiba et al. (1) with the exception of the phosphorylation rate (referred to as B1 in **Fig. 1A**) and those that have been newly introduced in this model (e.g. rates C2, C3 involved in the oxidation pathway). More specifically, the phosphorylation rate B1 is described by an expression similar to that used by Hashambhoy et al. (4), based on the assumption that a CaMKII monomer can be phosphorylated by an adjacent monomer from either side:

$$B1 = k_{cat} \cdot c_B \cdot \frac{CaMKII_{HoloAct}{}^2}{CaMKII_{HoloAct}{}^2 + k_T^2} \cdot \left(c_{Monomer(L)} + c_{Monomer(R)} \right)$$

In the above equation, c_B represents the activity coefficient associated with the active Ca^{2+}/CaM-bound conformational state (state B in **Fig. 1**) and $CaMKII_{HoloAct}$ represents the total activity of CaMKII holoenzyme in the dyad. The term $c_{Monomer(L)} + c_{Monomer(R)}$ describes the activities of neighboring subunits in the holoenzyme and the incorporation of the Hill-type term is essential as previously discussed in (4). Specifically, in the absence of this nonlinear term, the model predicts very fast dynamics in CaMKII autophosphorylation upon Ca^{2+}/CaM stimulation which are not in agreement with the experiments of De Koninck et al. (16). This indicates that there may be additional factors that influence the rate of CaMKII autophosphorylation within the holoenzyme. Hence, the empirical Hill-type function as discussed here may account for such cooperative and nonlinear interactions.

The oxidation dependent rate, k_{ox}(mM^{-1} ms^{-1}), is estimated using the dose-response activation of CaMKII by H_2O_2 as measured by Erickson et al. (17). Additionally, the reductase rate mediated by methionine sulfoxide reductase A (MsrA), k_{cat_MsrA} (ms^{-1}), is constrained using the oxidation dependent I_{CaL} facilitation data of Song et al. (15). All parameter values used in simulations are shown in **Tables S1** and **S2**.

Figure S1

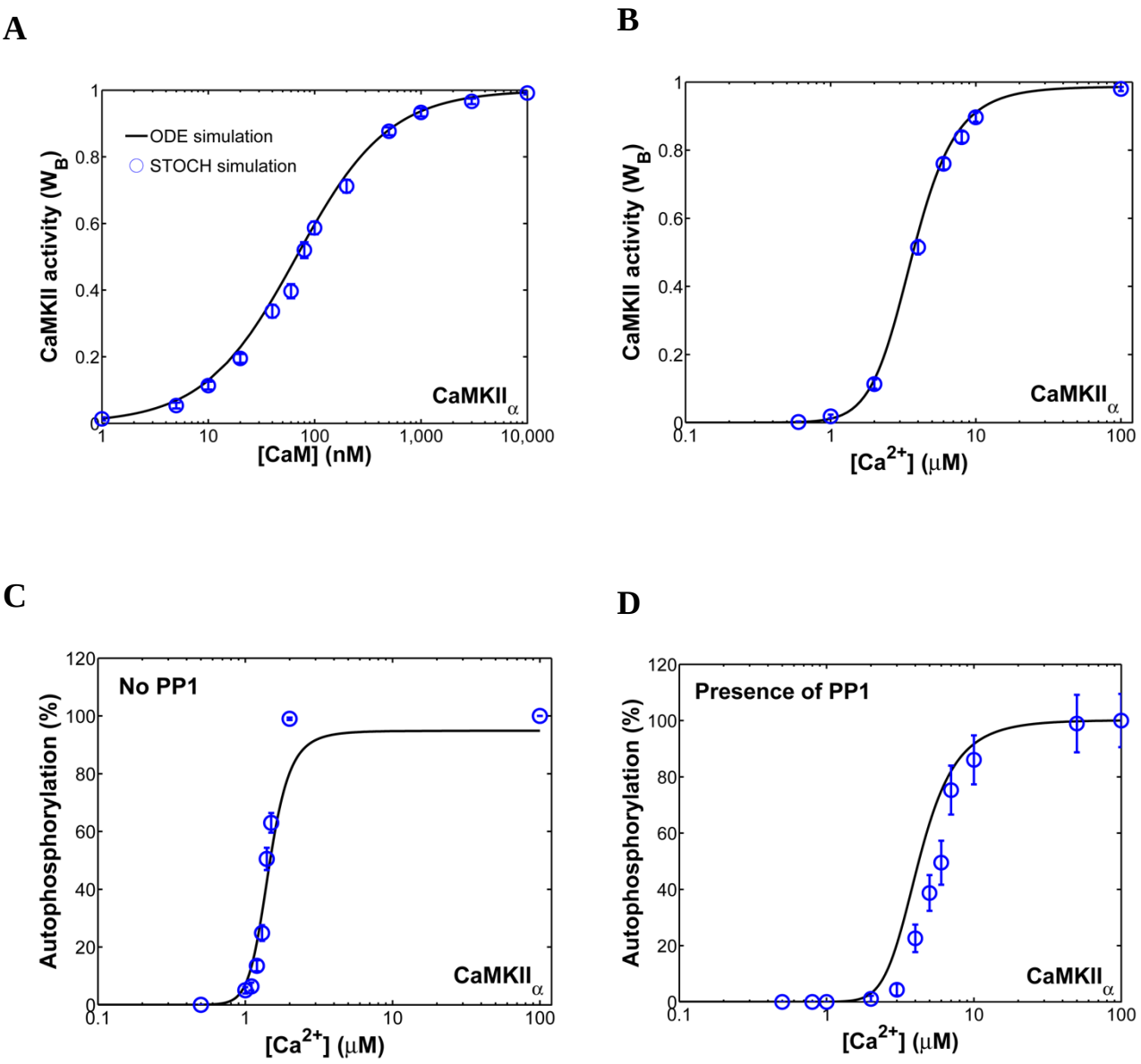

Figure S1. Stochastic simulations (STOCH, blue circles) using the proposed model compared to the deterministic simulations (ODE, solid lines) using the model of Chiba et al. (1) **(A, B)** Steady state activation of CaMKII by Ca^{2+}/CaM. These simulation data were generated under the following in vitro conditions: (A) 500 μM Ca^{2+} in the absence of ATP was incubated with different [CaM] (1-10,000 nM) for 1 min. The fraction of CaMKII subunits in the Ca^{2+}/CaM bound state (W_B), referred to as state B in Fig. 1A, is plotted against [CaM]; (B) In the absence of ATP and in the presence of different levels of [Ca^{2+}] (0.1-100 μM), CaMKII was incubated with 5 μM CaM for 1 min. **(C, D)** Relationship between the autophosphorylated level of CaMKIIα and [Ca^{2+}]. Experimental conditions used for simulations in panel C (absence of PP1): in the presence of 2mM ATP and different [Ca^{2+}] (0.1-100 μM), CaMKII was incubated with 50 μM CaM for 5 min at 0 ^{o}C. The percentage of CaMKII autophosphorylation is plotted against [Ca^{2+}]. Experimental conditions used for simulations in panel D (presence of PP1): in the presence of 2 mM ATP and different [Ca^{2+}], CaMKII and 1.25 μM PP1 were incubated with 5 μM CaM at 0 ^{o}C. The steady-state

value of the CaMKII autophosphorylation percentage (%) is plotted against [Ca^{2+}]. All stochastic simulations are averaged over 50 random iterations.

Figure S2

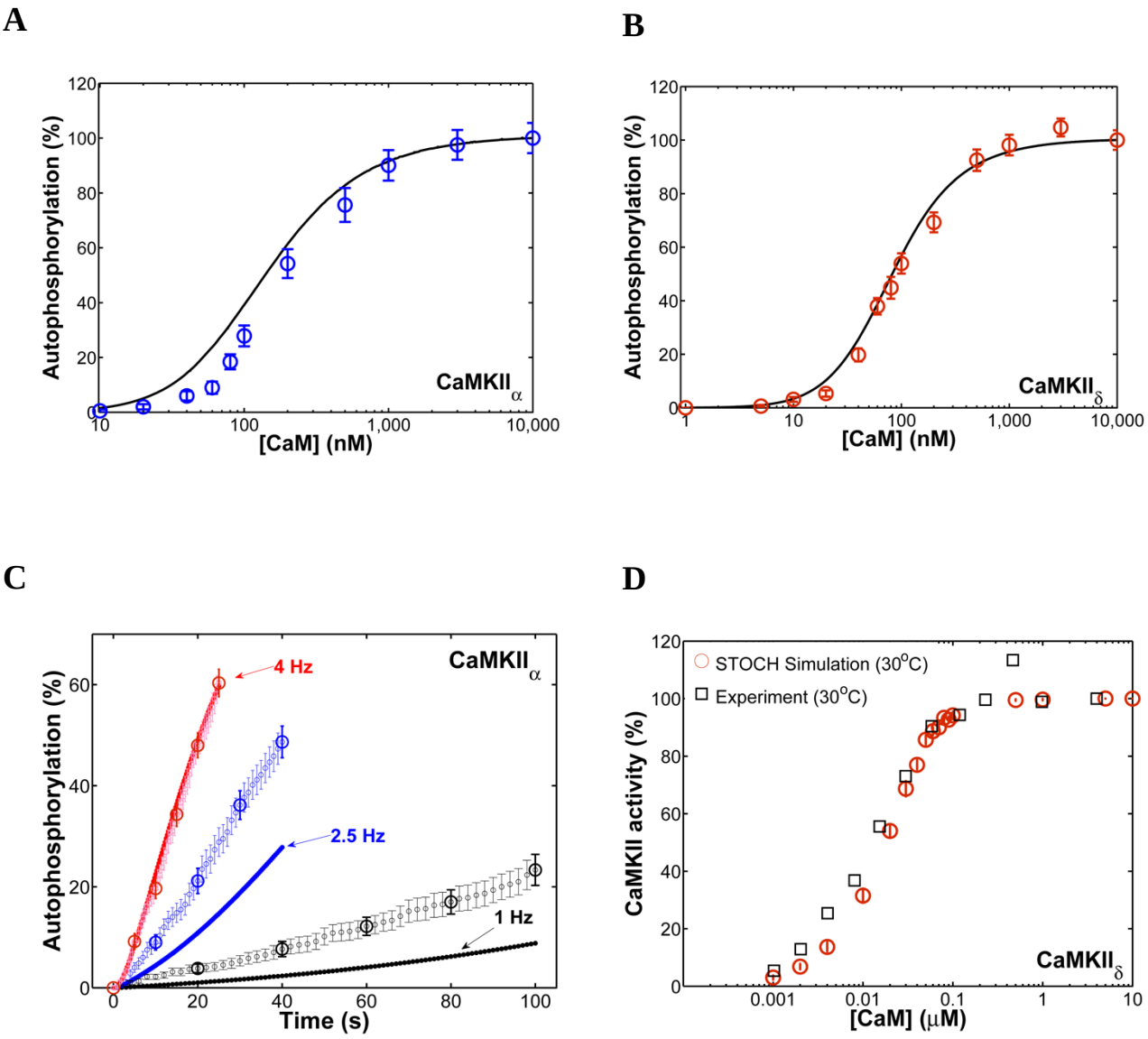

Figure S2. Relationship between [CaM] and the level of autophosphorylated CaMKII$_\alpha$ **(A)** and CaMKII$_\delta$ **(B)**. Simulation results (open circles) using the proposed stochastic model of CaMKII activation are compared to the deterministic simulations (solid lines) using the ODE model of Chiba et al. (1). Kinetic parameters of the stochastic model are appropriately adjusted to account for the molecular difference between the two isoforms (i.e. cardiac δ isoform has higher affinity for CaM compared to neuronal α isoform). **(C)** Frequency dependent activation of CaMKIIα. Experimental conditions used for simulations are taken from (18): The phosphorylation mixture (500 μM Ca^{2+}, 100 nM CaM and 0.25 mM ATP) was applied to CaMKIIα for 200 ms at different frequencies (open black circles, open blue circles, and open red circles represent 1, 2.5 and 4 Hz, respectively). Solid lines

represent simulation results using the CaMKII ODE model of Chiba et al. (1). **(D)** Dependence of $CaMKII_{\delta}$ activity on [CaM]. Experimental conditions used for simulations: $CaMKII_{\delta}$ was incubated with saturating Ca^{2+} (0.5 mM) and varying [CaM] for 1 min at 30 °C. Stochastic simulations (red circles) are compared to experimental data from (19).

Figure S3

A

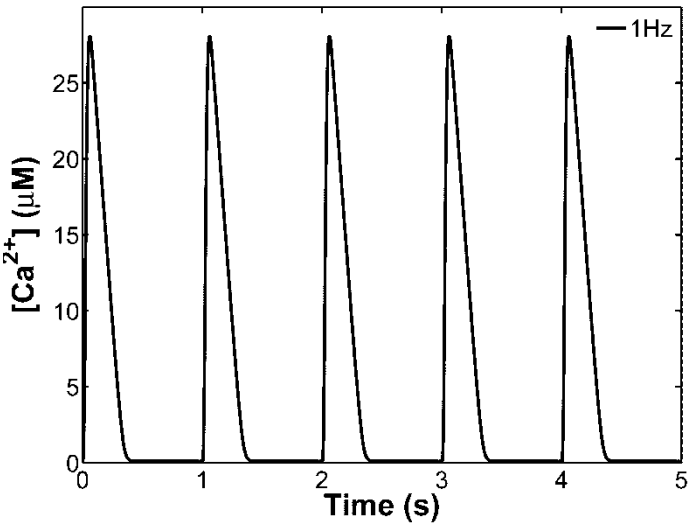

B

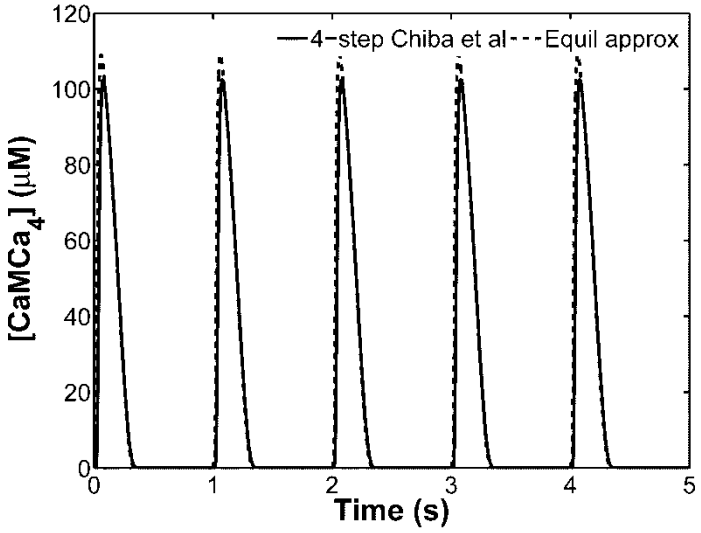

Figure S3. (A) Time course of the Ca^{2+} transient ($[Ca^{2+}]$) using the model of Chiba et al. (1) at a stimulus frequency of 1 Hz. **(B)** Simulation results for fully Ca^{2+}-bound CaM [$CaMCa_4$] obtained both with the four-step Ca^{2+} binding scheme of Chiba et al. (1) (solid lines) and the proposed simplified Ca^{2+}/CaM scheme (dashed lines).

Figure S4

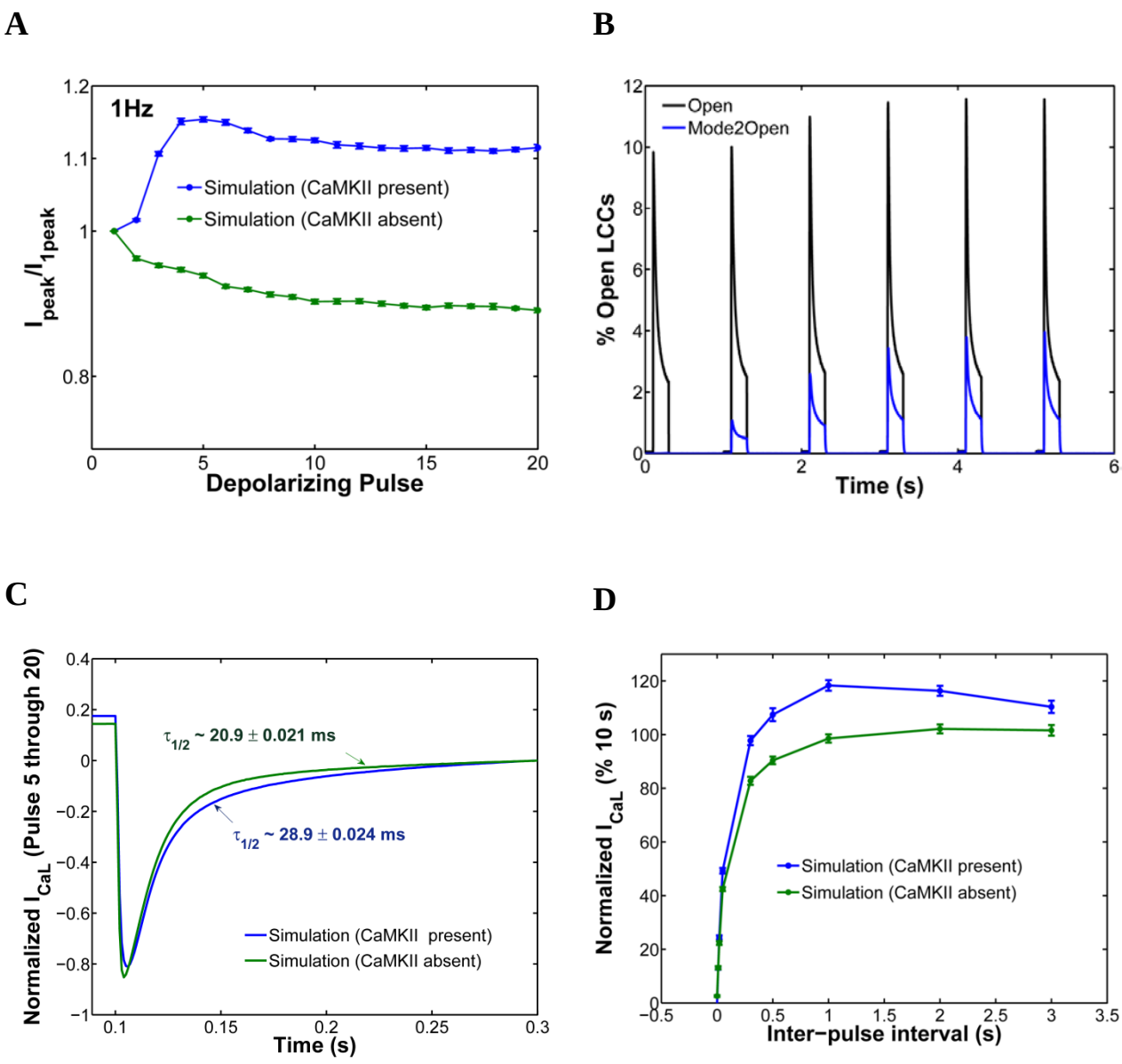

Figure S4. Ca^{2+}-dependent I_{CaL} facilitation mediated by CaMKII. **(A)** Normalized I_{CaL} amplitude during a 200-ms test pulse to 0 mV from -80 mV after a pre-pulse of -40 mV for 100 ms (1 Hz pacing stimulation). Two consecutive pulses were delivered consistent with the protocol employed by Hashambhoy et al. (4) and 20 random trials were performed for each experimental simulation (n = 20). Results in the presence (blue line) and absence (green line) of CaMKII are presented. **(B)** Simulated averaged percent of total LCCs that are open (black solid line) and percent of mode 2 LCCs that are open (blue line) under 1 Hz pacing protocol. **(C)** Average I_{CaL} (taken over 5^{th} to 20^{th} pulse) in the 1 Hz pacing protocol in the presence (blue solid line) and absence (green solid line) of CaMKII. Note the substantial slowing of macroscopic I_{CaL} inactivation due to shifts in modal distribution. **(D)** Simulated double pulse protocol in the presence and absence of CaMKII as employed by Hashambhoy et al. (4). I_{CaL} was measured as the difference between peak current and the residual current at the end of the pulse and normalized to peak I_{CaL} measured after a 10 s inter-pulse interval.

Figure S5

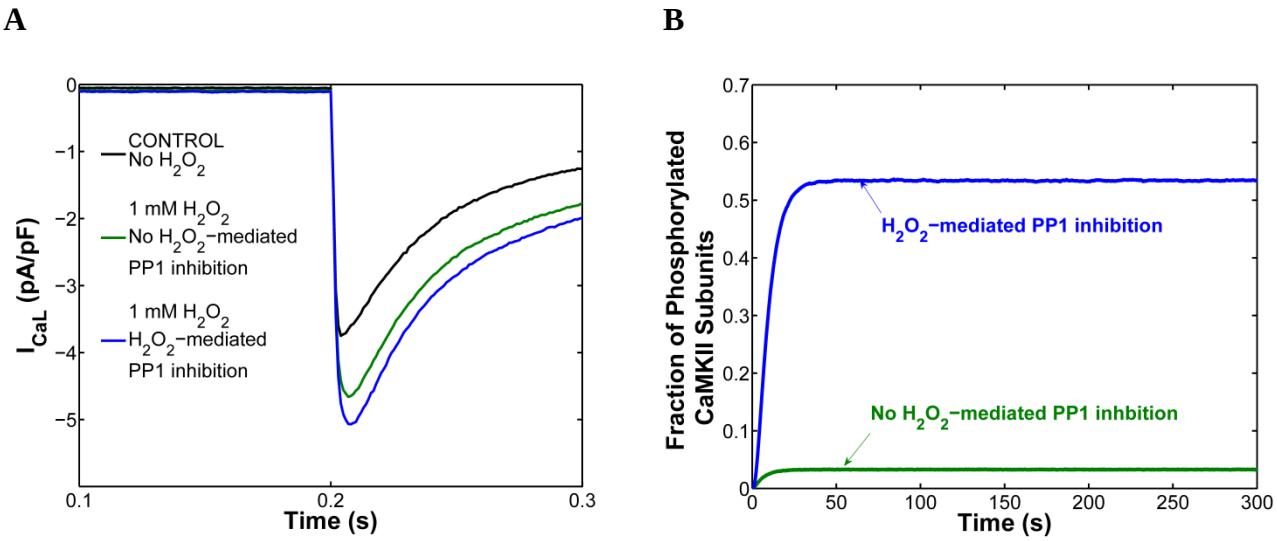

Figure S5. (A) Effects of H_2O_2 on I_{CaL}. I_{CaL} was simulated as recorded by Song et al. **(15)** by applying depolarizing voltage step pulses once every minute from a holding potential of -70 mV. Prior to a depolarization to 0 mV for 300 ms to activate I_{CaL}, Na^+ currents were inactivated by a pre-pulse to -40 mV for 200 ms. Before the application of H_2O_2, the model predicts peak I_{CaL} of 3.75 pA/pF (black line) with a half inactivation time ($\tau_{1/2}$) of ~30 ms. The application of 1 mM H_2O_2 increased both the peak amplitude of I_{CaL} and the average $\tau_{1/2}$ by ~ 24% (green lines). In the case where H_2O_2 is assumed to inhibit PP1 activity (K_{mROS} = 0.1 mM), the model predicts further increase in the peak amplitude of I_{CaL} (~35%) (blue line) compared to ~24% increase (green line) which is simulated in the absence of H_2O_2-mediated PP1 inhibition. In both cases, the simulated increase in I_{CaL} lies within the experimental range (26.0 ± 1.3%, 34.3 ± 3.9%) measured by Song et al. **(15)** during 5 min (acute) H_2O_2 exposure. **(B)** Effects of H_2O_2 on CaMKII autophosphorylation. Levels of phosphorylated CaMKII were simulated as measured by Song et al. **(20)** during exposure of resting myocytes to 1 mM H_2O_2 (5 min). In the case where H_2O_2 targets only CaMKII with no effect on PP1, the model predicts negligible CaMKII autophosphorylation (< 4 %). When these simulations are repeated in the presence of H_2O_2-mediated PP1 inhibition, the fraction of CaMKII subunits undergoing autophosphorylation (blue line) increases significantly.

Figure S6

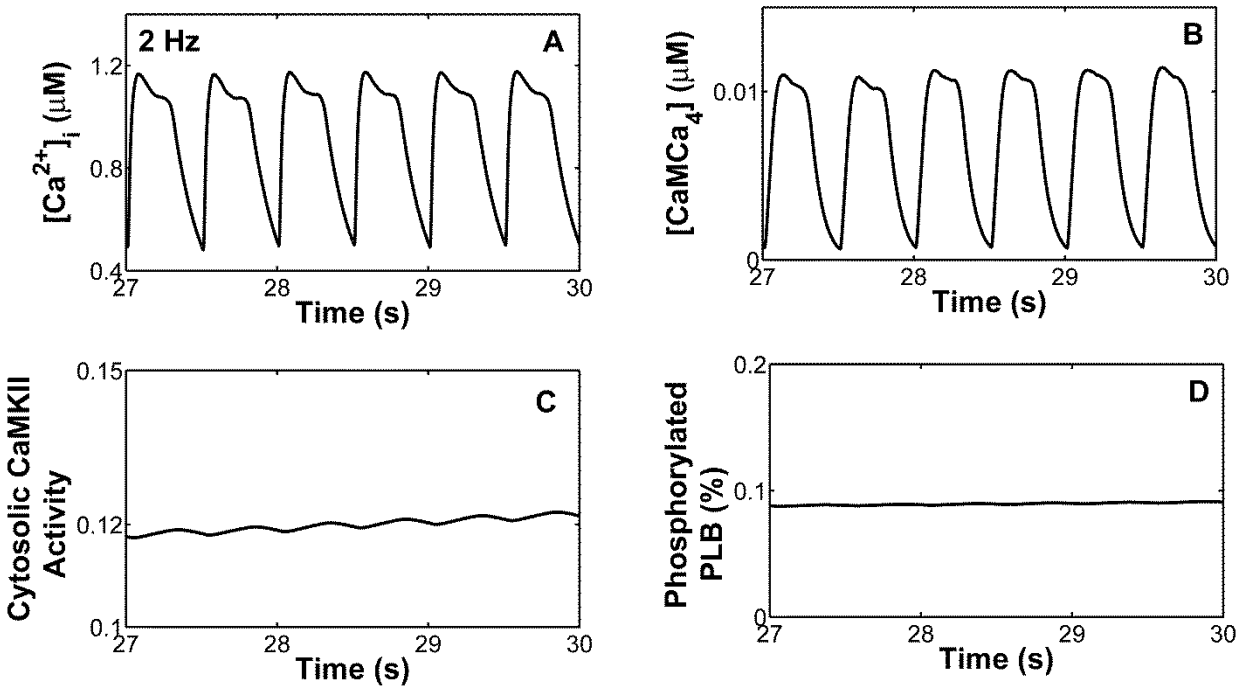

Figure S6. Predicted local dynamics in beating cardiac myocytes at 2Hz AP pacing: **(A)** Ca^{2+} transient ($[Ca^{2+}]_i$), **(B)** fully Ca^{2+}-bound CaM [$CaMCa_4$], **(C)** total (cytosolic) CaMKII activity and (D) PLB phosphorylation (%).

Figure S7

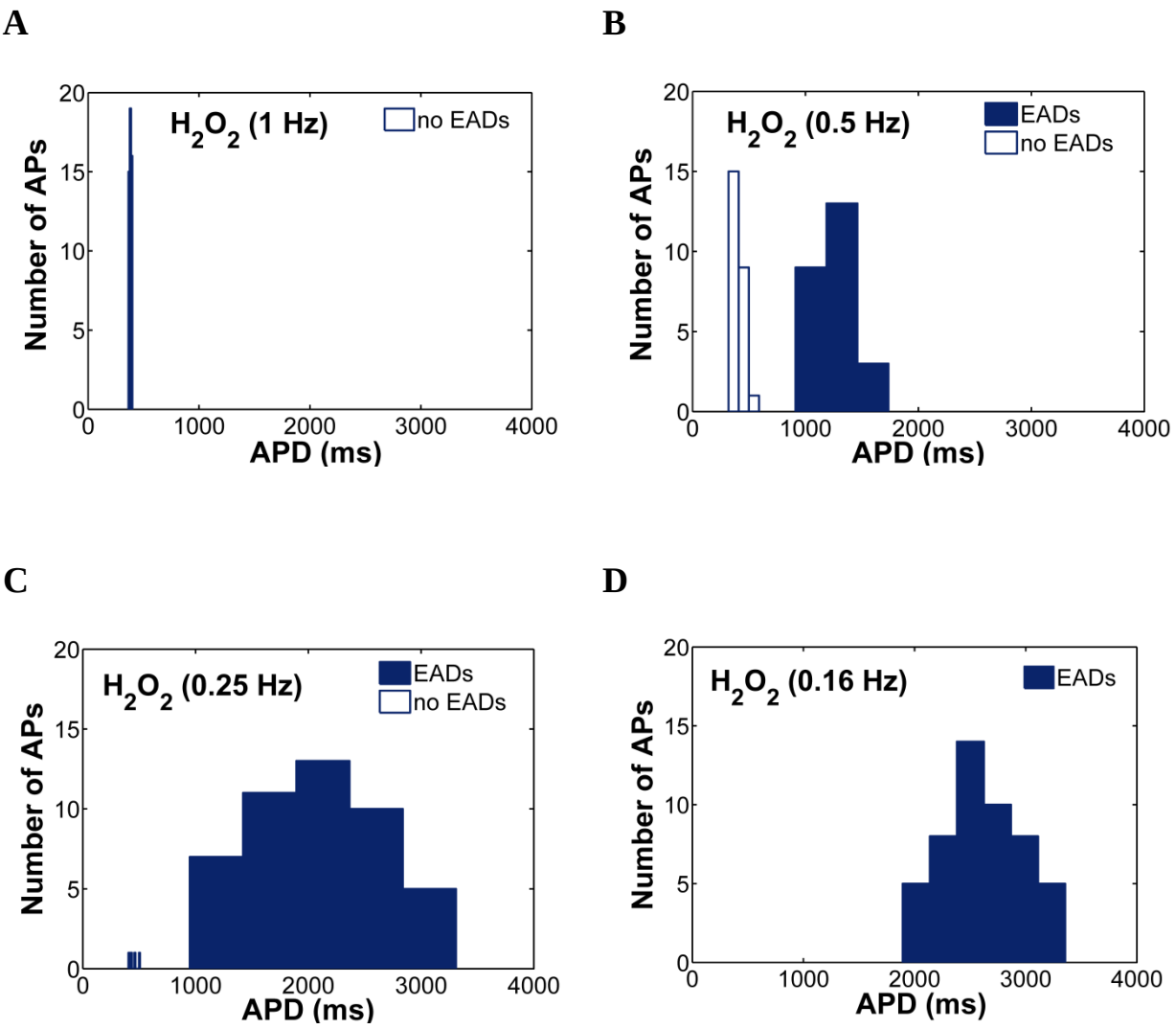

Figure S7. APD histograms under oxidative stress conditions and at various pacing frequencies (PCL ≥ 1 s). Open bars represent stable APs while filled bars represent EADs. AP pacing protocol simulations are performed at (A) 1 s PCL; (B) 2 s PCL; (C) 4 s PCL and (D) 6 s PCL.

Figure S8

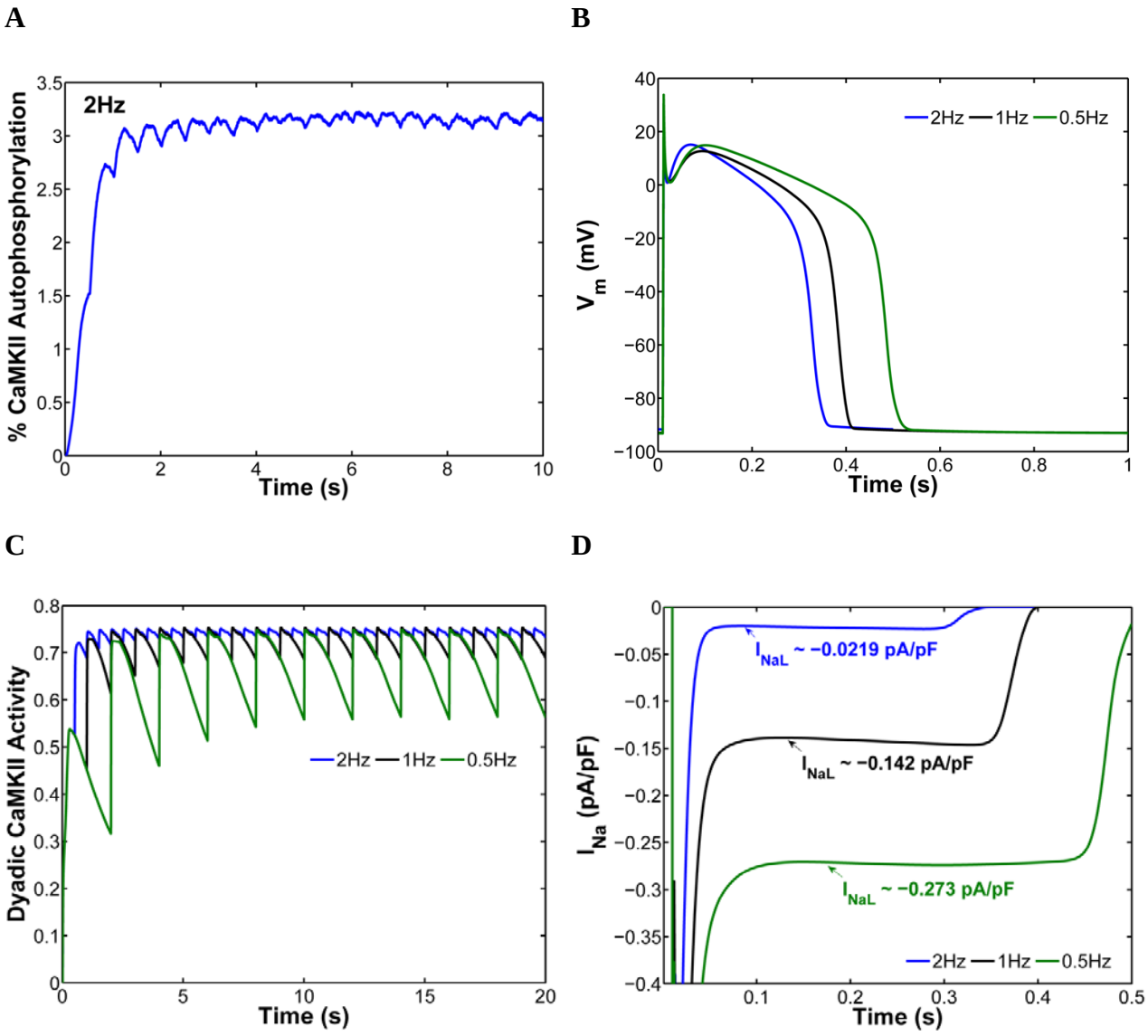

Figure S8. (A) Simulated CaMKII autophosphorylation at 2 Hz AP pacing protocol. **(B)** Steady-state APs simulated for PCLs of 500 (2Hz, blue), 1000 (1Hz, black) and 2000 (0.5Hz, green) ms. APD_{90} increases with PCL consistent with the experimental data of Li et al. **(21) (C, D)** Simulated rate-dependence of dyadic CaMKII activity and I_{NaL} under control conditions.

Figure S9

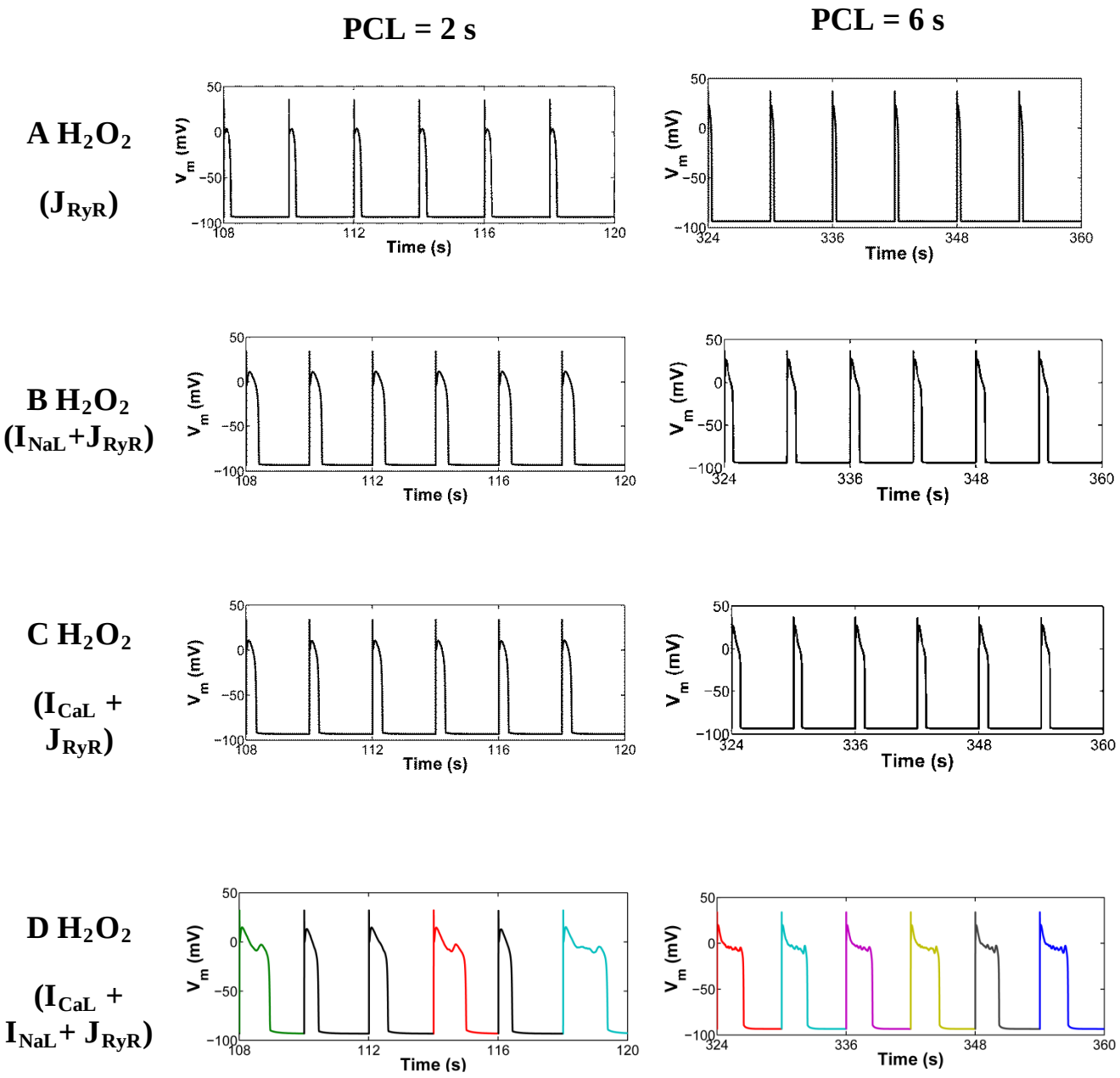

Figure S9. Simulated APs from both a 2 s and 6 s PCL pacing protocol in the presence of 200 µM H_2O_2 and under the assumption that CaMKII targets **(A)** only RyRs; **(B)** only Na^+ channels and RyRs; **(C)** only LCCs and RyRs; or **(D)** LCCs, RyRs and Na^+ channels.

Figure S10

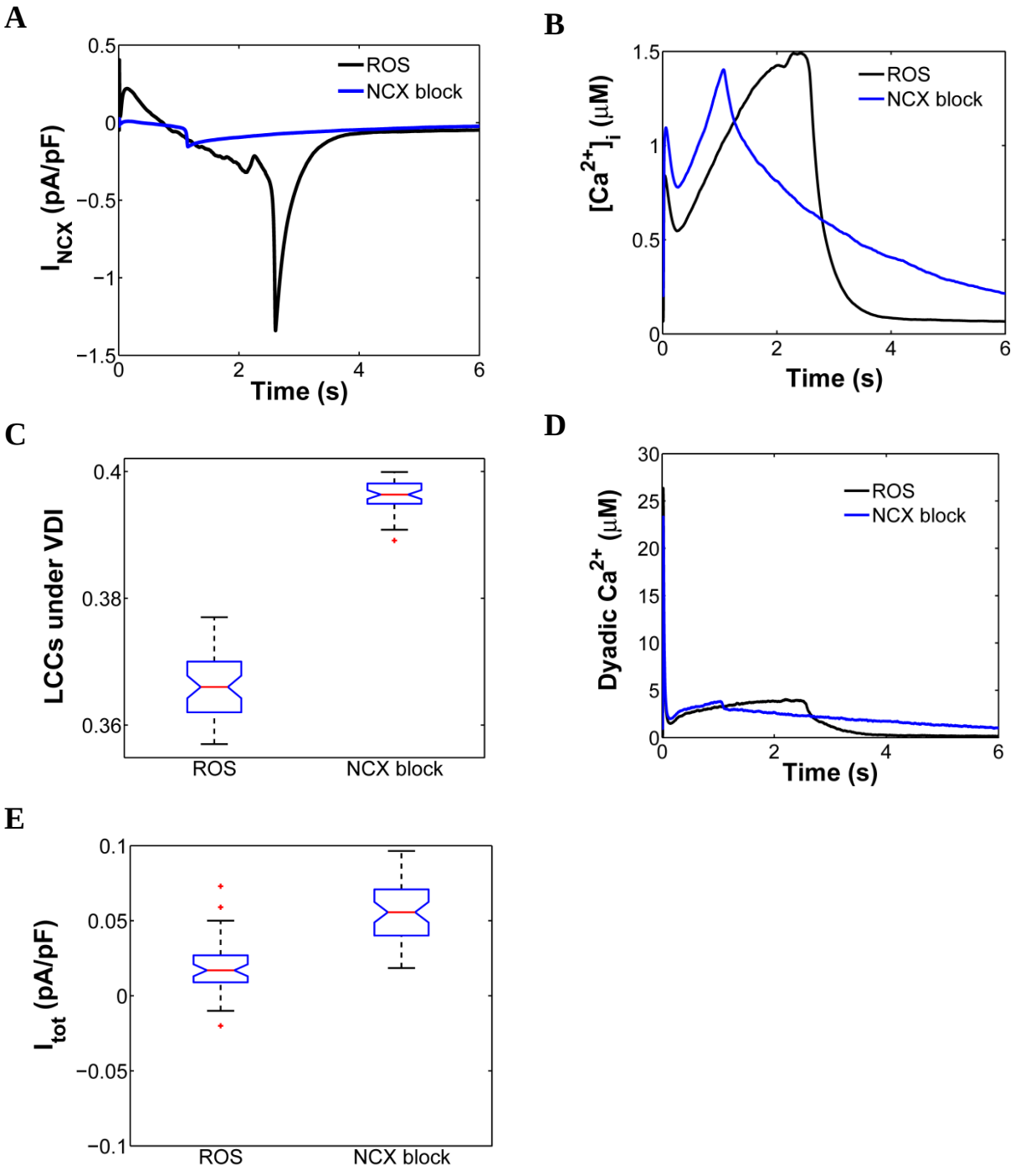

Figure S10. (A) Effects of oxidative stress (ROS, PCL = 6 s) on I_{NCX} before (ROS: black line) and after NCX inhibition (NCX block: blue line). **(B)** Simulated $[Ca^{2+}]_i$ at a PCL of 6 s under the same conditions. **(C)** Box plots of fraction of LCCs under VDI before and after NCX block. The latter is estimated at the time of NCX reversal. **(D)** Time course of dyadic $[Ca^{2+}]$ before and after NCX block. **(E)** Box plot of I_{tot} as measured at the time of NCX reversal before and after NCX block.

Figure S11

PCL = 2 s

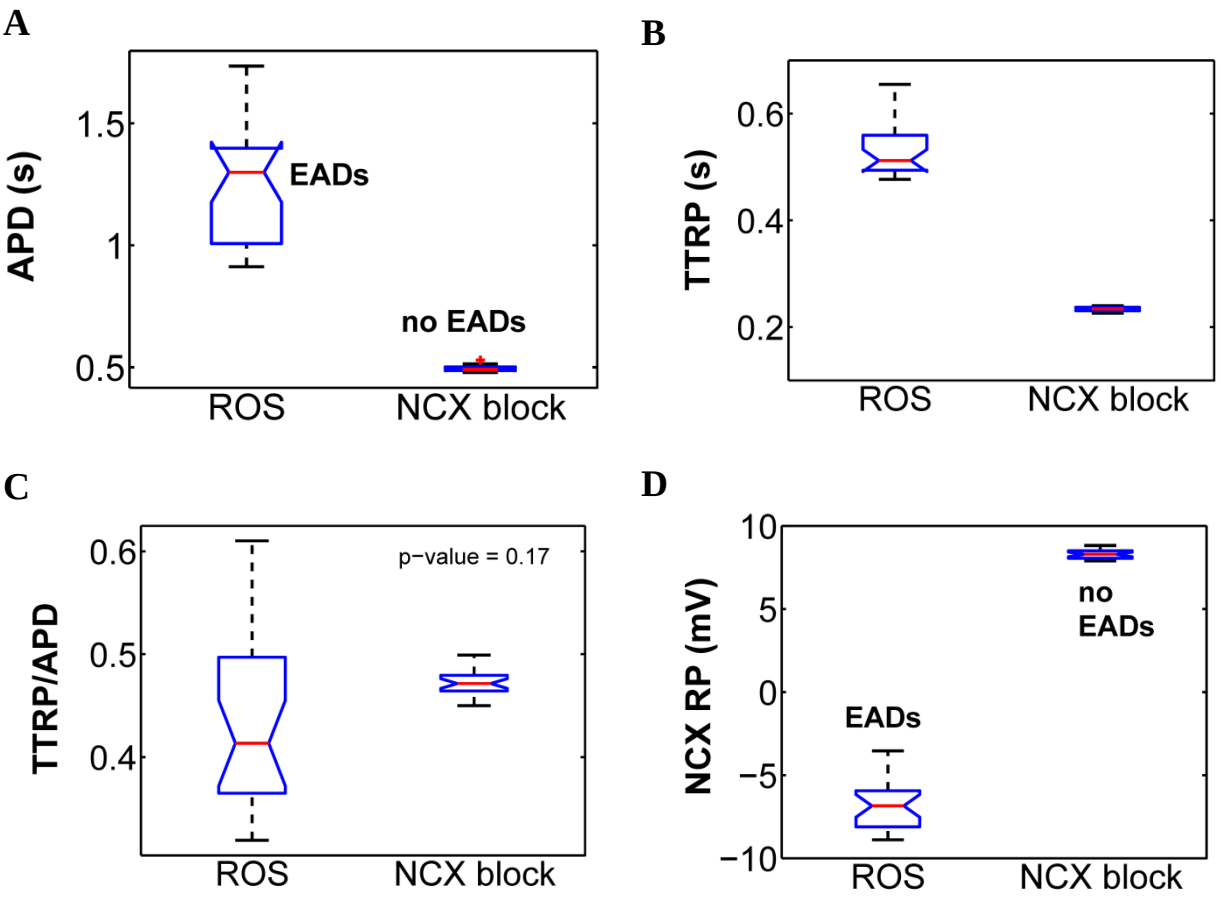

Figure S11. Box plots of **(A)** APD, **(B)** TTRP, **(C)** normalized TTRP (TTRP/APD) and **(D)** NCX RP before (ROS) and after NCX block during a 2 s PCL pacing protocol.

Figure S12

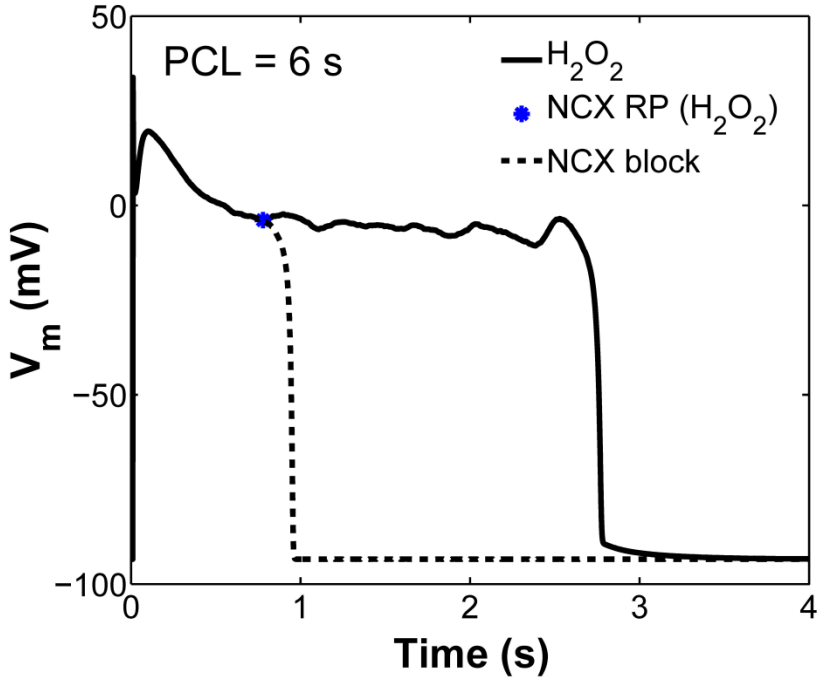

Figure S12. Simulated APs from a 6 s PCL pacing protocol under the presence of oxidative stress (200 μM H_2O_2) before (solid line) and after NCX block (dashed line). Note that NCX is blocked at the moment it reverses to forward mode in the presence of H_2O_2 (blue asterisk) and maintained for only 200 ms.

Figure S13

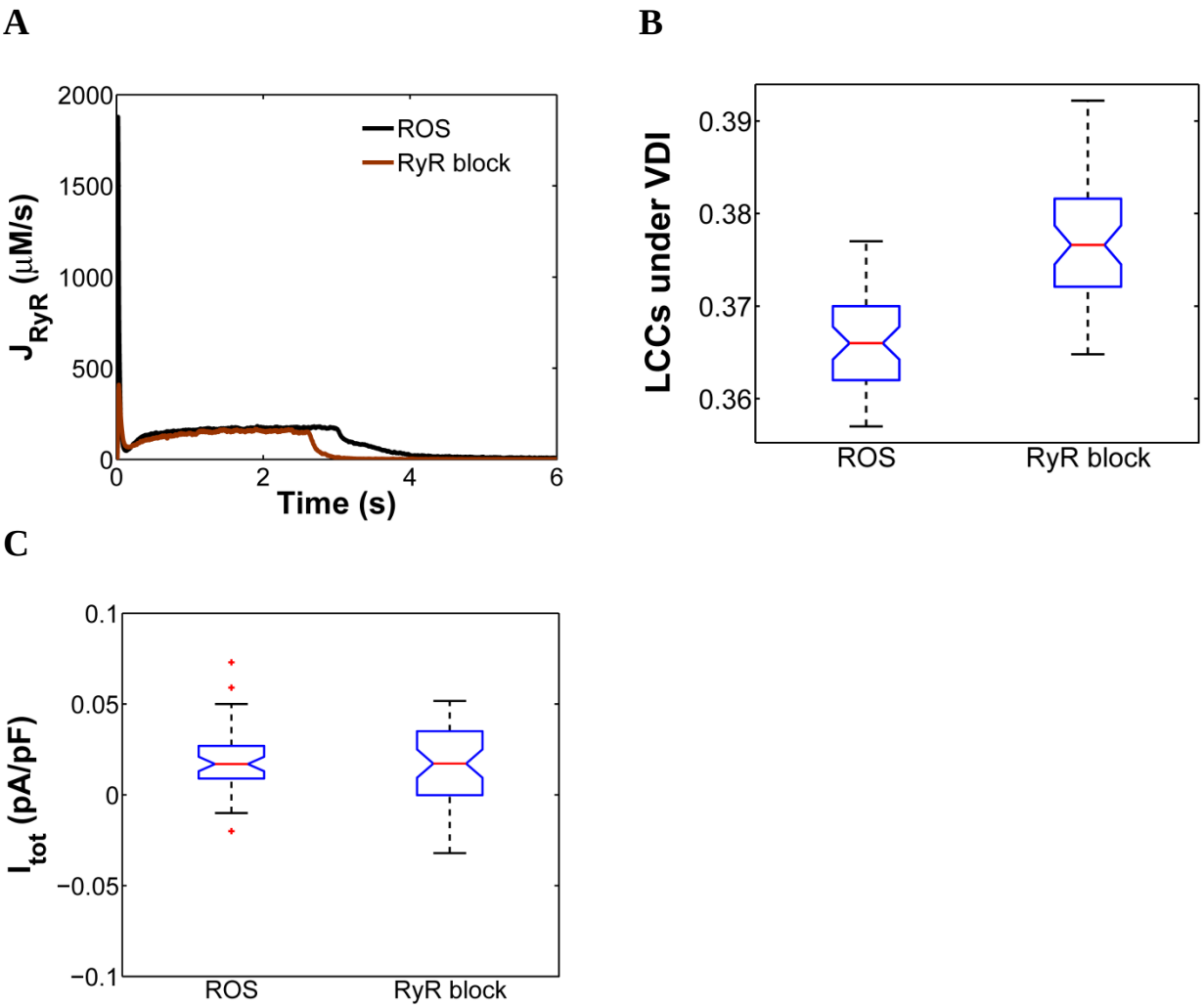

Figure S13. (A) Dynamics of SR Ca^{2+} release flux (J_{RyR}) before and after RyR block. As expected, RyR inhibition significantly decreases J_{RyR} by ~ 80%. **(B)** Box plot of fraction of LCCs that are not undergoing VDI – estimated at the time of NCX reversal – under the same conditions **(C)** Box plot of I_{tot} as measured at the time of NCX reversal before and after RyR inhibition.

Figure S14

A $[Na^+]_i$ = 12 mM

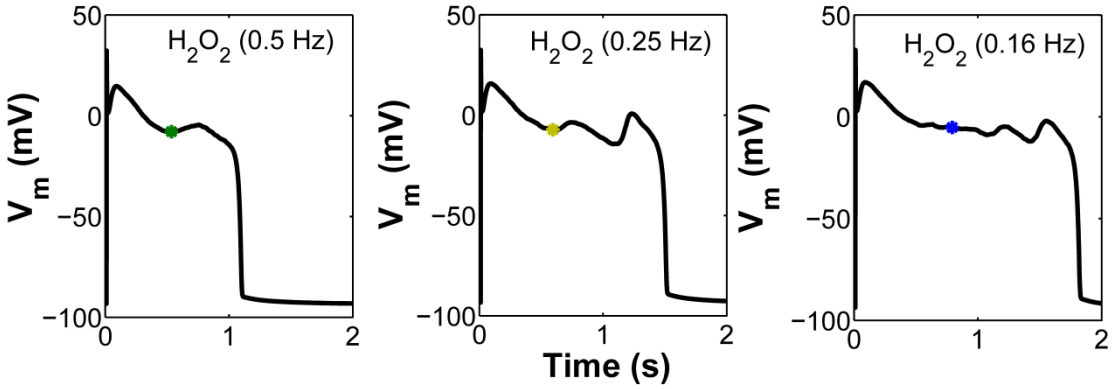

B

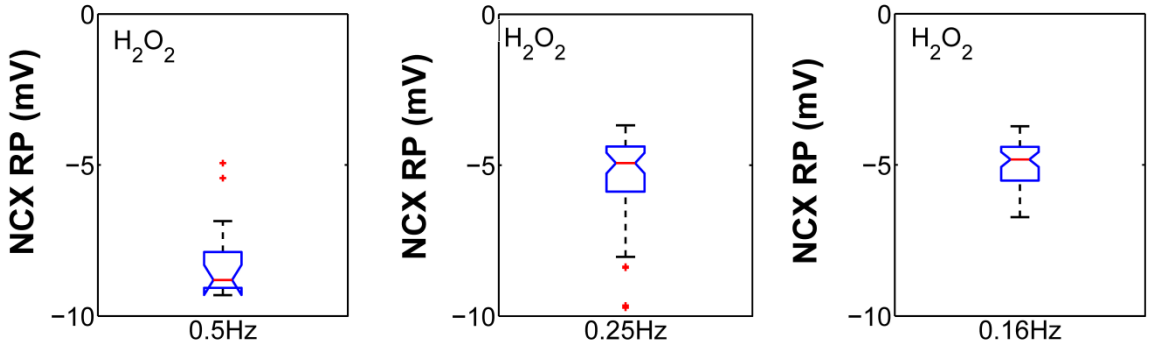

C

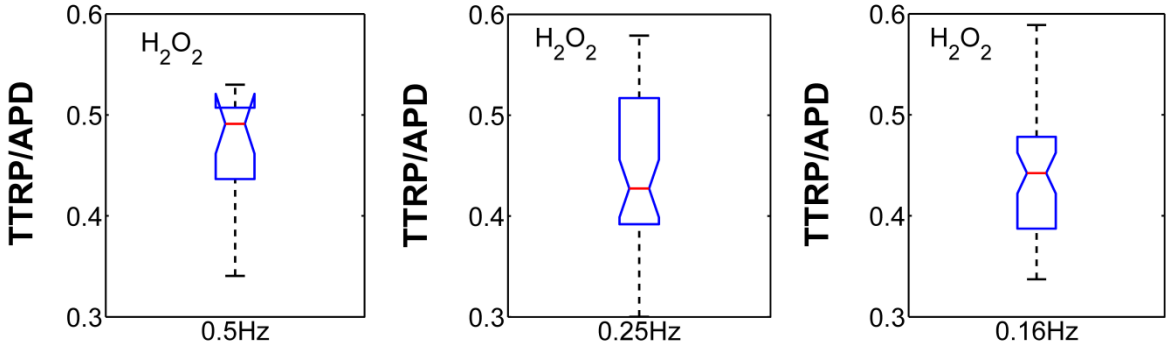

Figure S14. (A) Simulated EADs in the presence of oxidative stress (H_2O_2) at low pacing rates (PCL ≥ 2 s) with $[Na^+]_i$ = 12 mM. The moment that membrane potential crosses the NCX reversal potential is marked with colored asterisks. **(B, C)** Box plots of the NCX RP and normalized TTRP (TTRP/APD) for all H_2O_2–induced EADs with $[Na^+]_i$ = 12 mM.

Figure S15

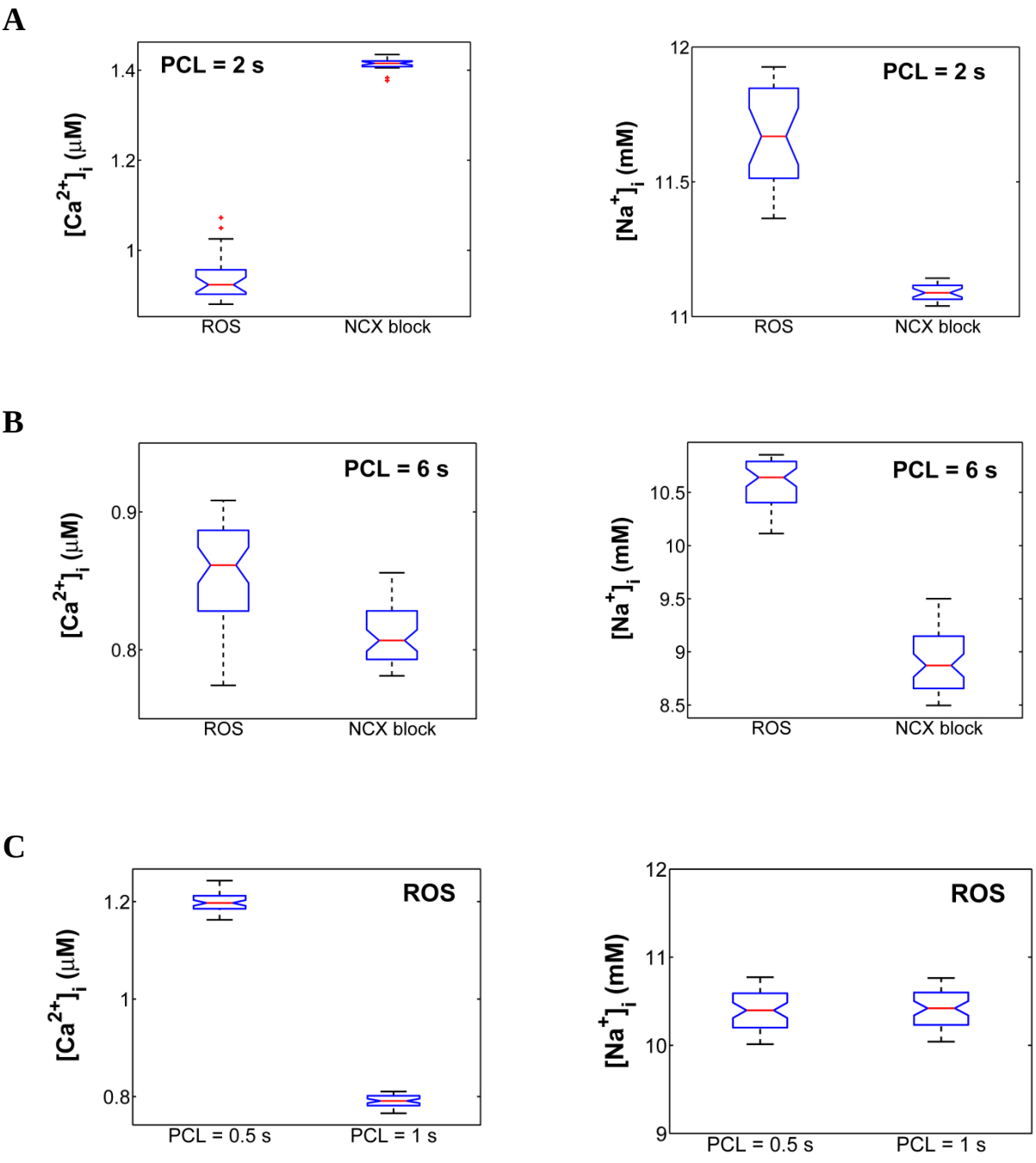

Figure S15. (A, B) Box plots of $[Ca^{2+}]_i$ and $[Na^+]_i$ as measured at the time of NCX reversal before (ROS) and after NCX block at a PCL of 2 s and 6 s. **(C)** Box plots $[Ca^{2+}]_i$ and $[Na^+]_i$ as measured at the time of NCX reversal in the presence of ROS and at fast pacing rates (PCL $\leq$ 1 s) where no EADs occur.

Figure S16

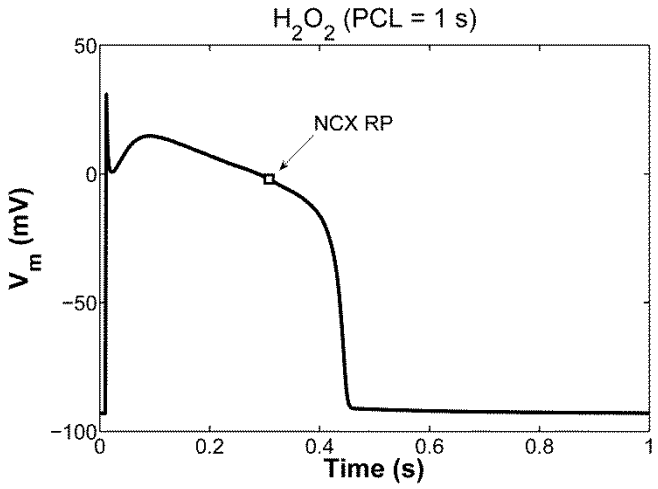

Figure S16. Simulated stable AP in the presence of ROS at a PCL of 1 s. Note that the NCX RP is marked with an open square.

Figure S17

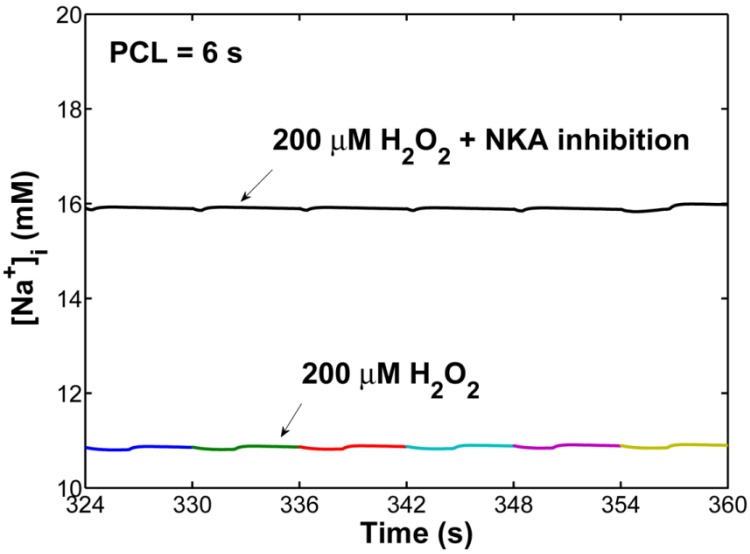

Figure S17. Effects of NKA inhibition on intracellular [Na^+] in the presence of 200 μM H_2O_2.

Figure S18

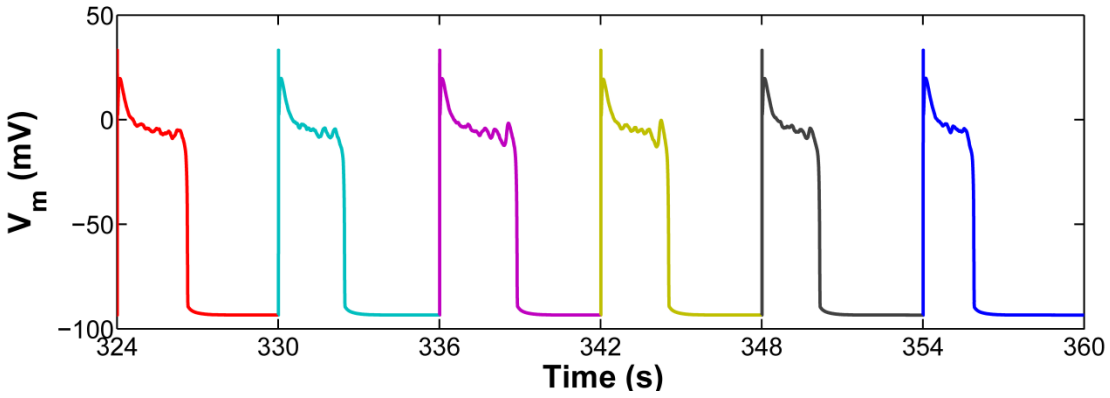

Figure S18. Simulated APs, all of which exhibit EADs for a 6 s PCL pacing protocol, under conditions of elevated oxidative stress (200 μM H_2O_2) including the full range of experimentally observed changes in I_{Na} properties as seen with CaMKII overexpression; including a shift in steady-state inactivation and a slowing of recovery from inactivation. Relevant I_{Na} model parameters (referred to as P_{1b5}, P_{1b6} and P_{1a7} in the model of Grandi et al. (11)) were adjusted to the values reported by Grandi et al. (11) for CaMKII overexpression.

Supplemental Tables

Table S1: Model parameters of the stochastic CaMKII activation model

Parameter	Value		Reference
	α isoform	**δ isoform**	
$[CaM]_{dyad}$	0.2 mM		(4)
$[PP1]_{dyad}$	0.096 mM		(22)
$[CaMKII]_{dyad}$	0.120 mM		(22)
k_1	$2.5\ mM^{-1}\ ms^{-1}$		(1)
k_{-1}, k_{-2}	$0.05\ ms^{-1}$		(1)
k_2	$88.25\ mM^{-1}\ ms^{-1}$		(1)
k_3	$12.5\ mM^{-1}\ ms^{-1}$		(1)
k_{-3}, k_{-4}	$1.25\ ms^{-1}$		(1)
k_{asso}	$5.34\ mM^{-1}\ ms^{-1}$		Model fit
$k_{\_disso}$	$4.36 \times 10^{-4}\ ms^{-1}$	$1.62 \times 10^{-4}\ ms^{-1}$	Model fit
$k_{\_dissoCa}$	$4.4 \times 10^{-3}\ ms^{-1}$	$1.6 \times 10^{-3}\ ms^{-1}$	Model fit
$k_{\_disso2}$	$4.36 \times 10^{-7}\ ms^{-1}$	$1.62 \times 10^{-7}\ ms^{-1}$	Model fit
$k_{\_dissoCa2}$	$4.4 \times 10^{-6}\ ms^{-1}$	$1.62 \times 10^{-6}\ ms^{-1}$	Model fit
k_{cat} (at 0^oC)	$4.17 \times 10^{-4}\ ms^{-1}$	$4.8 \times 10^{-4}\ ms^{-1}$	Model fit
k_{cat} (at $30\ ^oC$)	$2.4 \times 10^{-3}\ ms^{-1}$	$6.9 \times 10^{-4}\ ms^{-1}$	Model fit*
k_T	3.3		Model fit
k_{ox}	$0.0128\ mM^{-1}\ ms^{-1}$		Model fit
k_{MsrA}	$1.0 \times 10^{-4}\ ms^{-1}$		Model fit
K_{mCaM}	3.0×10^{-5} mM		(1)
K_{mATP}	19.1×10^{-3} mM		(1)
k_{cat_PP1}	$1.72 \times 10^{-3}\ ms^{-1}$		(1)
K_{m_PP1}	11.0×10^{-3} mM		(1)

[*]The value of parameter k_{cat} is further adjusted to scale for a difference in temperature. Based on the Arrhenius plot of Bradshaw et al. (23), k_{cat} at 37 ^{o}C is ~ 2-fold greater than k_{cat} at 30 ^{o}C. Considering the case for δ isoform, k_{cat} (at 37 ^{o}C) = 1.4 x 10^{-3} ms^{-1} (value used in whole-cell simulations).

Table S2: Cytosolic $CaMKII_{\delta}$ ODE model parameters for whole-cell simulations. Reaction rates for the phosphorylation dependent pathway are identical to those of Chiba et al. (1).

Parameter	**Value**	**Reference**
	δ isoform	
$[CaM]_{cyt}$	50 µM	(24)
$[PP1]_{cyt}$	14.3 µM	(4)
$[CaMKII]_{cyt}$	3.159 nM	(4)
k_1	2.5 mM^{-1} ms^{-1}	(1)
k_{-1}, k_{-2}	0.05 ms^{-1}	(1)
k_2	88.25 mM^{-1} ms^{-1}	(1)
k_3	12.5 mM^{-1} ms^{-1}	(1)
k_{-3}, k_{-4}	1.25 ms^{-1}	(1)
k_{asso}	2.1 mM^{-1} ms^{-1}	(1)
$k_{\_disso}$	0.7 x 10^{-4} ms^{-1}	(1)
$k_{\_dissoCa}$	0.95 x 10^{-3} ms^{-1}	(1)
$k_{\_disso2}$	0.7 x 10^{-7} ms^{-1}	(1)
$k_{\_dissoCa2}$	0.95 x 10^{-6} ms^{-1}	(1)
k_{cat} (at 37 ^{o}C)	2.0 x 10^{-4} ms^{-1}	Adjusted[1]
K_{mCaM}	3.0 x 10^{-5} mM	(1)
K_{mATP}	19.1 x 10^{-3} mM	(1)
k_{cat_PP1}	1.72 x 10^{-3} ms^{-1}	(1)
K_{m_PP1}	11.0 x 10^{-3} mM	(1)

[1]The parameter k_{cat} (at 37 ^{o}C) is estimated using the relevant data of Gaertner et al. (19) measured at 30 ^{o}C and then adjusted to body temperature using the Arrhenius plot of Bradshaw et al. (23).

Table S3: State variable initial conditions in the presence of 200 µM H_2O_2

Variable	PCL = 1 s	PCL = 2 s	PCL = 4 s	PCL = 6s
V_m (mV)	-92.896	-91.635	-92.922	-93.186
$[Ca^{2+}]_i$ (mM)	1.468×10^{-4}	5.452×10^{-4}	1.468×10^{-4}	7.179×10^{-5}
$[Ca^{2+}]_{JSR}$ (mM)	0.743	0.620	0.754	0.777
$[Ca^{2+}]_{dyad}$ (mM)	5.486×10^{-4}	1.629×10^{-3}	5.368E-04	2.035E-04
$[Ca]_{NSR}$ (mM)	0.754	0.651	0.765	0.779
$[Na^+]_i$ (mM)	10.051	11.231	10.155	10.134
$[K^+]_i$ (mM)	131.776	131.574	131.866	131.994
IC_3 (I_{Na})	0.052	0.046	0.053	0.055
IC_2 (I_{Na})	4.707×10^{-4}	5.151×10^{-4}	4.662×10^{-4}	4.419×10^{-4}
IF (I_{Na})	2.955×10^{-5}	6.085×10^{-5}	1.988×10^{-5}	1.459×10^{-5}
IM_1 (I_{Na})	0.229	0.505	0.150	1.363×10^{-3}
IM_2 (I_{Na})	0.024	0.135	0.022	4.824×10^{-5}
C_3 (I_{Na})	0.688	0.310	0.767	0.935
C_2 (I_{Na})	5.706×10^{-3}	2.948×10^{-3}	6.346×10^{-3}	7.516×10^{-3}
C_1 (I_{Na})	1.730×10^{-5}	1.044×10^{-5}	1.915×10^{-5}	2.194×10^{-5}
O (I_{Na})	9.301×10^{-9}	8.881×10^{-9}	9.650×10^{-9}	9.698×10^{-9}
LC_3 (I_{Na})	1.532×10^{-4}	6.621×10^{-4}	1.562×10^{-4}	4.433×10^{-4}
LC_2 (I_{Na})	1.270×10^{-6}	6.285×10^{-6}	1.292×10^{-6}	3.563×10^{-6}
LC_1 (I_{Na})	3.832×10^{-9}	2.193×10^{-9}	3.885×10^{-9}	1.039×10^{-8}
LO (I_{Na})	0.0	0.0	0.0	0.0
x_{Ks} (IK_s)	2.339×10^{-4}	2.656×10^{-3}	1.779×10^{-4}	1.720×10^{-4}
[LTRPNCa] (mM)	0.133	0.364	0.133	0.067
[HTRPNCa] (mM)	0.986	0.995	0.985	0.960
C_O ($I_{Kv4.3}$)	0.957	0.957	0.957	0.957
C_1 ($I_{Kv4.3}$)	0.023	0.025	0.023	0.022

C_2 ($I_{Kv4.3}$)	2.009 x 10^{-4}	2.426 x 10^{-4}	2.002 x 10^{-4}	1.924 x 10^{-4}
C_3 ($I_{Kv4.3}$)	7.927 x 10^{-7}	1.053 x 10^{-6}	7.881 x 10^{-7}	7.425 x 10^{-7}
O ($I_{Kv4.3}$)	1.173 x 10^{-9}	1.714 x 10^{-9}	1.164 x 10^{-9}	1.074 x 10^{-9}
CI_O ($I_{Kv4.3}$)	0.015	0.015	0.015	0.015
CI_1 ($I_{Kv4.3}$)	4.614 x 10^{-3}	5.102 x 10^{-3}	4.606 x 10^{-3}	4.514 x 10^{-3}
CI_2 ($I_{Kv4.3}$)	7.095 x 10^{-4}	8.638 x 10^{-4}	7.069 x 10^{-4}	6.790 x 10^{-4}
CI_3 ($I_{Kv4.3}$)	5.743 x 10^{-5}	7.698 x 10^{-5}	5.711 x 10^{-5}	5.376 x 10^{-5}
OI ($I_{Kv4.3}$)	8.716 x 10^{-7}	7.995 x 10^{-7}	6.966 x 10^{-7}	5.469 x 10^{-7}
CO ($I_{Kv1.4}$)	0.679	0.419	0.771	0.859
C_1 ($I_{Kv1.4}$)	0.083	0.057	0.094	0.102
C_2 ($I_{Kv1.4}$)	3.798 x 10^{-3}	2.957 x 10^{-3}	4.295 x 10^{-3}	4.557 x 10^{-3}
C_3 ($I_{Kv1.4}$)	7.733 x 10^{-5}	6.769 x 10^{-5}	8.724 x 10^{-5}	9.034 x 10^{-5}
O ($I_{Kv1.4}$)	5.948 x 10^{-7}	5.991 x 10^{-7}	6.666 x 10^{-7}	6.716 x 10^{-7}
CI_O ($I_{Kv1.4}$)	0.215	0.470	0.120	0.031
CI_1 ($I_{Kv1.4}$)	0.012	0.029	6.523 x 10^{-3}	1.665 x 10^{-3}
CI_2 ($I_{Kv1.4}$)	4.632 x 10^{-3}	0.013	2.568 x 10^{-3}	6.403 x 10^{-4}
CI_3 ($I_{Kv1.4}$)	1.783 x 10^{-3}	5.522 x 10^{-3}	9.861 x 10^{-4}	2.395 x 10^{-4}
OI ($I_{Kv1.4}$)	1.134 x 10^{-3}	3.939 x 10^{-3}	6.233 x 10^{-4}	1.448 x 10^{-4}

†Initial values for APs are obtained at each PCL following 10 beats (steady state). We would like to clarify that the notion of "steady-state" for unstable APs (e.g. EADs) refers to the condition in which the SR Ca^{2+} cycles in a stable repeating pattern on a beat-to-beat basis. In the case of a 2 s PCL pacing protocol, steady state values are obtained following 60 beats.

Table S4: Parameters modified to simulate the block of a current or channels such as RyR

Intervention	**Parameter**	**WT value**	**Value (after block)**	**Definition**
I_{NaL} block	α_8	5.4 x 10^{-7} ms^{-1}	5.4 x 10^{-8} ms^{-1}	(11)
I_{CaL} block	α, β	8.0 x 10^{-4} ms^{-1}	8.0 x 10^{-5} ms^{-1}	(4)
I_{NCX} block	k_{NaCa}	0.27 pA pF^{-1}	0.27 x 10^{-1} pA pF^{-1}	(24)
J_{RyR} block	k_{oCa}	6500 mM^{-2} ms^{-1}	130 mM^{-2} ms^{-1}	(25)

Supporting References

1. Chiba, H., N. S. Schneider, S. Matsuoka, and A. Noma. 2008. A simulation study on the activation of cardiac CaMKII delta-isoform and its regulation by phosphatases. Biophys J 95:2139-2149.

2. Holmes, W. R. 2000. Models of calmodulin trapping and CaM kinase II activation in a dendritic spine. Journal of computational neuroscience 8:65-85.

3. Hashambhoy, Y. L., R. L. Winslow, and J. L. Greenstein. 2011. CaMKII-dependent activation of late INa contributes to cellular arrhythmia in a model of the cardiac myocyte. Conf Proc IEEE Eng Med Biol Soc 2011:4665-4668.

4. Hashambhoy, Y. L., R. L. Winslow, and J. L. Greenstein. 2009. CaMKII-induced shift in modal gating explains L-type Ca(2+) current facilitation: a modeling study. Biophys J 96:1770-1785.

5. Dzhura, I., Y. Wu, R. J. Colbran, J. R. Balser, and M. E. Anderson. 2000. Calmodulin kinase determines calcium-dependent facilitation of L-type calcium channels. Nat Cell Biol 2:173-177.

6. Yue, D. T., S. Herzig, and E. Marban. 1990. Beta-adrenergic stimulation of calcium channels occurs by potentiation of high-activity gating modes. Proceedings of the National Academy of Sciences of the United States of America 87:753-757.

7. Szabo, G., N. Szentandrassy, T. Biro, B. I. Toth, G. Czifra, J. Magyar, T. Banyasz, A. Varro, L. Kovacs, and P. Nanasi. 2005. Asymmetrical distribution of ion channels in canine and human left-ventricular wall: epicardium versus midmyocardium. Pflug Arch Eur J Phy 450:307-316.

8. Hua, F., and R. F. Gilmour, Jr. 2004. Contribution of IKr to rate-dependent action potential dynamics in canine endocardium. Circulation research 94:810-819.

9. Huke, S., and D. M. Bers. 2007. Temporal dissociation of frequency-dependent acceleration of relaxation and protein phosphorylation by CaMKII. Journal of molecular and cellular cardiology 42:590-599.

10. Guo, T., T. Zhang, R. Mestril, and D. M. Bers. 2006. Ca2+/Calmodulin-dependent protein kinase II phosphorylation of ryanodine receptor does affect calcium sparks in mouse ventricular myocytes. Circ Res 99:398-406.

11. Grandi, E., J. L. Puglisi, S. Wagner, L. S. Maier, S. Severi, and D. M. Bers. 2007. Simulation of Ca-calmodulin-dependent protein kinase II on rabbit ventricular myocyte ion currents and action potentials. Biophys J 93:3835-3847.

12. Wagner, S., N. Dybkova, E. C. Rasenack, C. Jacobshagen, L. Fabritz, P. Kirchhof, S. K. Maier, T. Zhang, G. Hasenfuss, J. H. Brown, D. M. Bers, and L. S. Maier. 2006. Ca2+/calmodulin-dependent protein kinase II regulates cardiac Na+ channels. The Journal of clinical investigation 116:3127-3138.

13. Wagner, S., H. M. Ruff, S. L. Weber, S. Bellmann, T. Sowa, T. Schulte, M. E. Anderson, E. Grandi, D. M. Bers, J. Backs, L. Belardinelli, and L. S. Maier. 2011. Reactive oxygen species-activated Ca/calmodulin kinase IIdelta is required for late I(Na) augmentation leading to cellular Na and Ca overload. Circ Res 108:555-565.

14. O'Loghlen, A., M. I. Perez-Morgado, M. Salinas, and M. E. Martin. 2003. Reversible inhibition of the protein phosphatase 1 by hydrogen peroxide. Potential regulation of eIF2 alpha phosphorylation in differentiated PC12 cells. Arch Biochem Biophys 417:194-202.

15. Song, Y. H., H. Cho, S. Y. Ryu, J. Y. Yoon, S. H. Park, C. I. Noh, S. H. Lee, and W. K. Ho. 2010. L-type Ca(2+) channel facilitation mediated by H(2)O(2)-induced activation of CaMKII in rat ventricular myocytes. Journal of molecular and cellular cardiology 48:773-780.

16. De Koninck, P., and H. Schulman. 1998. Sensitivity of CaM kinase II to the frequency of Ca2+ oscillations. Science 279:227-230.

17. Erickson, J. R., M. L. Joiner, X. Guan, W. Kutschke, J. Yang, C. V. Oddis, R. K. Bartlett, J. S. Lowe, S. E. O'Donnell, N. Aykin-Burns, M. C. Zimmerman, K. Zimmerman, A. J. Ham, R. M. Weiss, D. R. Spitz, M. A. Shea, R. J. Colbran, P. J. Mohler, and M. E. Anderson. 2008. A dynamic pathway for calcium-independent activation of CaMKII by methionine oxidation. Cell 133:462-474.

18. De Koninck, P., and H. Schulman. 1998. Sensitivity of CaM kinase II to the frequency of Ca2+ oscillations. Science 279:227-230.

19. Gaertner, T. R., S. J. Kolodziej, D. Wang, R. Kobayashi, J. M. Koomen, J. K. Stoops, and M. N. Waxham. 2004. Comparative analyses of the three-dimensional structures and enzymatic properties of alpha, beta, gamma and delta isoforms of Ca2+-calmodulin-dependent protein kinase II. J Biol Chem 279:12484-12494.

20. Yoon, J. Y., W. K. Ho, S. T. Kim, and H. Cho. 2009. Constitutive CaMKII activity regulates Na+ channel in rat ventricular myocytes. Journal of molecular and cellular cardiology 47:475-484.

21. Li, G. R., C. P. Lau, A. Ducharme, J. C. Tardif, and S. Nattel. 2002. Transmural action potential and ionic current remodeling in ventricles of failing canine hearts. American journal of physiology. Heart and circulatory physiology 283:H1031-1041.

22. Soltis, A. R., and J. J. Saucerman. 2010. Synergy between CaMKII substrates and beta-adrenergic signaling in regulation of cardiac myocyte Ca(2+) handling. Biophys J 99:2038-2047.

23. Bradshaw, J. M., A. Hudmon, and H. Schulman. 2002. Chemical quenched flow kinetic studies indicate an intraholoenzyme autophosphorylation mechanism for Ca2+/calmodulin-dependent protein kinase II. The Journal of biological chemistry 277:20991-20998.

24. Greenstein, J. L., and R. L. Winslow. 2002. An integrative model of the cardiac ventricular myocyte incorporating local control of Ca2+ release. Biophys J 83:2918-2945.

25. Shannon, T. R., F. Wang, J. Puglisi, C. Weber, and D. M. Bers. 2004. A mathematical treatment of integrated Ca dynamics within the ventricular myocyte. Biophys J 87:3351-3371.